JOURNAL OF MATERIALS SCIENCE 24 (1989) 2739–2745

Analysis of the d.c. and a.c. properties of K_2O-doped porous $Ba_{0.5}Sr_{0.5}TiO_3$ ceramic humidity sensor

Y. C. YEH, T. Y. TSENG
Institute of Electronics, College of Engineering, National Chiao-Tung University, Hsinchu 30039, Taiwan, Republic of China

A humidity sensor using K_2O-doped porous $Ba_{0.5}Sr_{0.5}TiO_3$ ceramic is investigated. This ceramic humidity sensor exhibits a porous structure. The porous ceramic easily absorbs water vapour throughout the pores. The log-conductance against relative humidity (r.h.) sensitivity of this sensor is greater than 4 orders of magnitude in the range of 15 ~ 95% r.h. at 400 Hz and 25° C. The adsorption process of the sensor is very fast. Its adsorption response time in r.h. variation from 15 to 95% is within a few seconds. Charging–discharging and complex impedance analysis techniques are used to analysis the direct current (d.c.) and alternating current (a.c.) response of this device under 50 ~ 95% r.h. The sample can be polarized like electrolytes on charging process due to electrode space charge and grain surface water molecular polarization effects. The degree of polarization is enhanced with increasing r.h. The conduction carriers of this sensor in a humid atmosphere are ions and electrons, and the dominant conduction carrier is the ion. Using complex impedance analysis techniques, an equivalent circuit model associated with "non-Debye" capacitance is built. This model separates the sample into three regions: crystal grain, grain surface and electrode surface. The grain surface resistance and electrode surface resistance decrease sharply with increasing r.h., but crystal grain resistance is not affected by water vapour.

1. Introduction

Some porous metal oxides can be used as ceramic humidity sensor materials [1-3]. Generally, they are more chemically and thermally stable than other moisture sensing materials. The sensing mechanism is that adsorption of the surrounding water vapours can enhance the surface electrical conductivity and dielectric constant of metal oxides [4, 5]. Due to this the relative humidity (r.h.) variation can be converted into electrical signal variation through a ceramic humidity sensor. A ceramic humidity sensor can be easily installed in electronic equipment to detect or control the ambient moisture content.

According to the conduction carrier, the porous metal oxide humidity sensor can be classified into two types, electronic and ionic. Shimizu *et al.* [6] showed that perovskite-type oxides can be used as humidity sensing material at high temperature (300 ~ 400° C) and that its dominant conduction carrier in moisture and high temperature atmosphere is the electron. Sadaoka *et al.* [2] showed that KH_2PO_4-doped porous PLZT (Pb, La) (Zr, Ti) O_3 can be used as a humidity sensing device at room temperature (30° C) and its dominant carrier is the ion (proton).

It is to be pointed out elsewhere [7] that porous perovskite-type $Ba_{0.5}Sr_{0.5}TiO_3$ can be used as humidity sensing material. Its dominant humidity sensing carrier at room temperature (25° C) is the positive ion (probably proton). In this report, we further investigate this kind of material doped with various molar percentages of potassium oxide. It is found that the conductance–humidity sensitivity of this new device can be increased about ten times larger than the previous compact manufactured by sintering pure $Ba_{0.5}Sr_{0.5}TiO_3$ at 1200° C. The adsorption response time of this new sensor to r.h. variation from 15 to 95% is a few seconds.

For detailed analysis the inner electrical conduction behaviour of the sample under different r.h., both d.c. and a.c. measurement methods are used. The d.c. current against time curves measured on charging and discharging processes can be used to identify whether the conduction carrier is an ion, electron or both. It can also be used to determine which one is the dominant carrier. The measured a.c. data can be used to plot the complex planes. Analysing the complex plane diagrams can help in building the equivalent circuit models. It is found that complex impedance plots are most useful for analysing this device under 65 ~ 95% r.h. The complex impedance plots of the sample at 65 ~ 95% r.h. exhibit inclined semicircles with their centres depressed below the real axis at higher frequencies and have spurs at lower frequencies. These kind of inclined semicircles do not follow the Debye theory and can not be modelled by using an equivalent circuit with ideal capacitance and ideal resistance.

These "non-Debye" behaviour is also observed for many solid ionics and dielectrics, and can be well modelled using equivalent circuit associated with dispersive and frequency dependent "non-Debye" capacitance, which is proposed by Jonscher [8, 9]. Using this concept an equivalent circuit model associated with "non-Debye" capacitance is constructed to discuss the effect of water vapour on the inner electrical conduction behaviour of the sample.

2. Experimental procedure

The mixing powders were prepared by ball milling preweighed portions of reagent-grade $BaTiO_3$, $Sr(OH)2 \cdot 8H_2O$, TiO_2 and K_2CO_3 in acetone for 20 h. These mixing powders were dried and prereacted in air at 1100° C for 2 h, remilled, redried and seived through a 140 mesh screen to produce the starting powders with a composition of $Ba_{0.5}Sr_{0.5}TiO_3$–$(K_2O)_x$. The starting powders were then pressed into disks with a diameter of 10 mm and thickness of 2 mm. The pressed disks were placed on platinum crucible to sinter in air at 1250° C for 1 h. The sintered compact was termed the BSK sample.

The microstructure of the sample was examined by scanning electron micrograph (SEM). The average grain size was determined by the linear intercept technique from a micrograph of the sample fracture surface as shown in Fig. 1. The specific surface area was determined by the BET method using nitrogen gas. The fired bulk density and open porosity were obtained by Archimedes techniques.

For electrical measurement, gold electrodes were applied to opposite faces of the sample by a vacuum evaporation method. The a.c. electrical parameters, conductance $G(\omega)$ and susceptance $B(\omega)$, of the sample were measured by an impedance analyser (5 ~ 13 MHz) which was automatically controlled by a computer. The d.c. current against time curves of the sample were obtained by picoamperemeter which was also automatically controlled by a computer. The ambient atmosphere of temperature and humidity were controlled by temperature/humidity controllable test chamber.

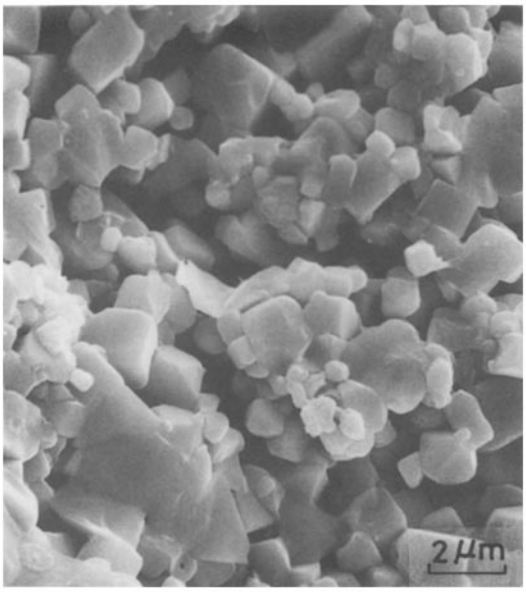

Figure 1 Scanning electron micrograph of fracture surface of the BSK sintered compact.

3. Results and discussion

3.1. Device characteristics

The structural characteristics of the sintered compacts manufactured by sintering pure $Ba_{0.5}Sr_{0.5}TiO_3$ oxide at 1200° C (BS1) and K_2O-doped $Ba_{0.5}Sr_{0.5}TiO_3$ oxide at 1250° C (BSK) are summarized in Table I. The conductance against humidity sensitivity of BS1 and BSK devices measured at 25° C and 1 V a.c. (400 Hz) is depicted in Fig. 2. The two curves in Fig. 2 have a good linear relationship between log-conductance and r.h., and can be expressed as

$$G(r.h.) = G_0 \exp (m \times r.h.) \qquad (1)$$

where G_0 is the conductance of the sensor at 25° C and 15% r.h. and m is the slope of the log-conductance against r.h. curve. From Fig. 2, it can be calculated out that m is 12.0 for BSK sample and 8.9 for BS1 sample. From Table I and Fig. 2, it is found that specimen BS1 has larger open porosity and specific surface area than specimen BSK, hence BS1 sample will have a larger adsorption surface and space than the BSK sample, yet the conductance-humidity sensitivity of BSK sample is about ten times larger than the BS1 sample. It may be attributed to the effect that doping potassium oxide can create more surface defect sites or oxygen vacancies on metal oxide surface, and defect sites or oxygen vacancies at metal oxide surface can increase the activated sites for water vapour adsorption [10, 11].

The desorption and adsorption response time curves of the BSK sample measured at 1 V a.c. (400 Hz) in various r.h. from 95 to 15% and from 15 to 95% are shown in Fig. 3. The adsorption process of the sample is very fast. The adsorption response time of this sensor in r.h. variation from 15 to 95% is within a few

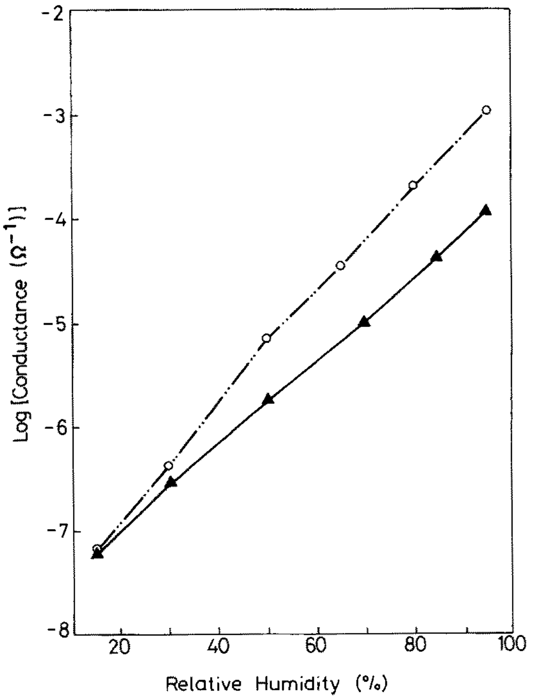

Figure 2 Log conductance against r.h. characteristic curves at 1V a.c. (400 Hz) for BSK specimen (○) and BS1 specimen (▲).

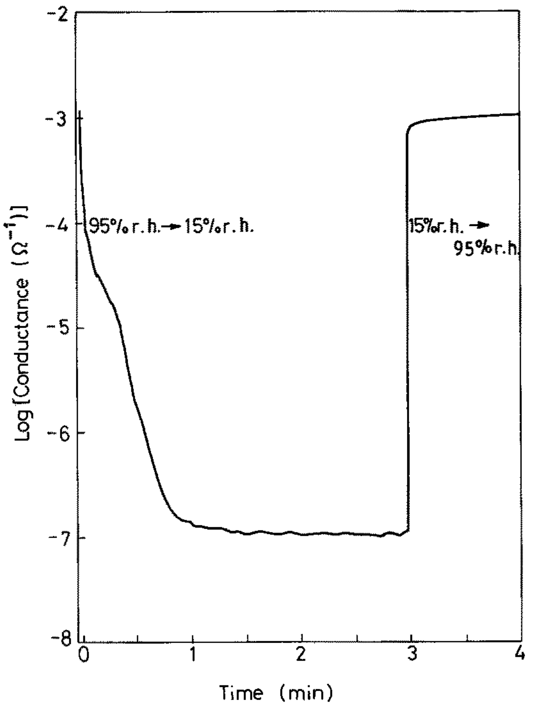

Figure 3 The desorption and adsorption response time curve of BSK sensor in r.h. variations from 95 to 15% and from 15 to 95%.

seconds, yet its desorption response time in r.h. variation from 95% to 15% is about 1 min. By subtracting the time required to set the r.h. into a desired value, the desorption response time is less than 1 min.

3.2. d.c. analysis

Figure 4 depicts the charging and discharging curves of BSK sample measured at 1 V d.c., 65% r.h. and 25° C. When 1 V d.c. voltage is applied at the sample, the sample can be polarized like electrolytes, and the current exponentially decays from an initial value of 17 μA to a final steady state value of 0.28 μA. At the end of the charging time, the applied voltage is changed to 0 V automatically by a program control. The removing of external applied voltage causes current to change direction, and a discharging current exponentially decays from an initial value of $-17.5\,\mu$A to a final steady state value of $-0.05\,\mu$A. Because the gold electrodes are blocking electrodes for mobile ions, which can block ions supplied at an electrode or discharged at an electrode. Thus the source of polarization is mobile ions which are impeded by the blocking electrode and accumulated at electrode interfaces. This kind of polarization is called space charge polarization which appears as in increase in capacitance as far as the exterior circuit is concerned [2]. Space charge polarization, in general, has relaxation times longer than ionic and electronic polarizations, and participates only at lower frequencies.

TABLE I Structural characteristics of BS1 and BSK sintered compacts

Specimen No.	Relative density (% theoretical)	Open porosity (% theoretical)	Average grain size (μm)	Specific surface area (m^2 g^{-1})
BS1	64	31	0.6	0.95
BSK	74	22	1.2	0.37

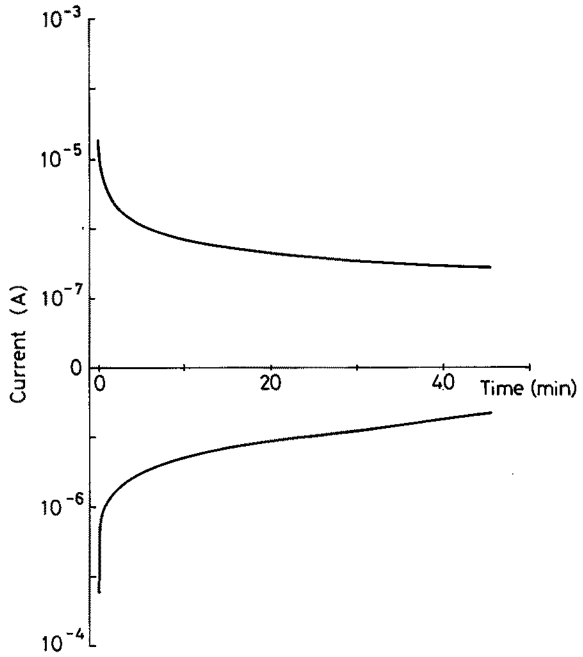

Figure 4 Charging and discharging curves of BSK sample at 1V d.c. for r.h. (■) 50%; (▲) 65%; (○) 80%; (●) 95%.

The variation of charging current with time can be represented by single relaxation time model [12]. During the charging process, assuming the rate of change of charge with time is proportional to the difference between its final value and its actual value

$$\frac{d(Q_{tc} - Q_{ic})}{dt} = \frac{1}{\tau_c}[(Q_{\infty c} - Q_{ic}) - (Q_{tc} - Q_{ic})] \quad (2)$$

then

$$Q_{tc} - Q_{ic} = (Q_{\infty c} - Q_{ic})\left(1 - \exp\left[\frac{-t}{\tau_c}\right]\right) \quad (3)$$

and

$$I_c(t) = \frac{dQ_t}{dt} = \left(\frac{Q_{\infty c} - Q_{ic}}{\tau_c}\right)\exp\left[\frac{-t}{\tau_c}\right] \quad (4)$$

where Q_{tc} is the actual accumulated charge on interfaces at time t, Q_{ic} is the instantaneous accumulated charge on applied field (if there is no accumulated charge on interfaces before the field is applied, then Q_{ic} is zero), $Q_{\infty c}$ is the final accumulated charge at the end of charging time, and τ_c is a charging relaxation time. If Q_{ic} is zero, then during charging process, the initial and final current can be written as follows

$$I_c(0) = \frac{Q_{\infty c}}{\tau_c} \quad (5)$$

and

$$I_c(\infty) = 0 \quad (6)$$

If the conduction carrier of the sample is only the ion, then from Equation 6 the value of $I_c(\infty)$ must be zero. But the final steady state current measured at the end of charging time is 0.28 μA not zero. This means that the conduction carriers of the sample are ions and electrons. The ion carriers are accumulated at

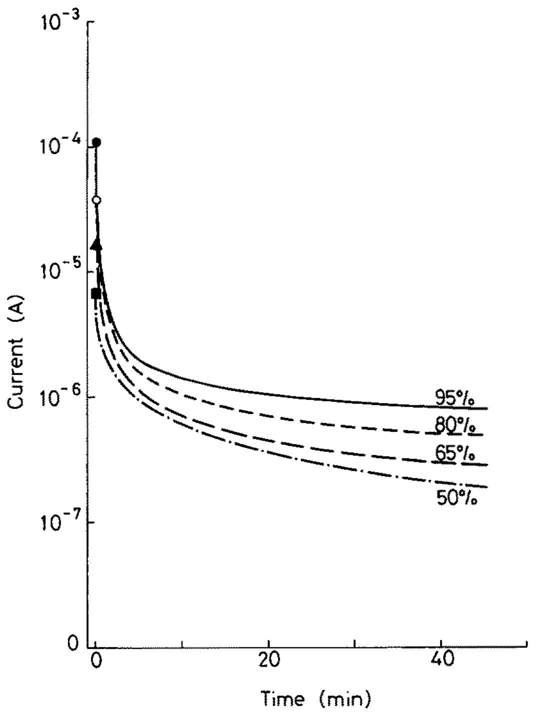

Figure 5 Charging curves of BSK sample at 1V d.c. and 50 ~ 95% r.h.

electrode interfaces and contribute a charging current $I_c(t)$, but the electron carriers can pass through the interfaces and contribute a steady state current I_s. Thus the total current, I_{tc}, of the sample on charging process can be written as

$$\begin{aligned} I_{tc}(t) &= I_c(t) + I_s \\ &= \left(\frac{Q_{\infty c} - Q_{ic}}{\tau_c}\right) \exp\left[\frac{-t}{\tau_c}\right] + \frac{V}{R} \end{aligned} \qquad (7)$$

where V is the applied voltage (1V), and R is a resistance which is a measure of electron conductivity of the sample.

When the applied voltage is removed, the discharging current can be expressed as

$$I_d(t) = \frac{dQ_{td}}{dt} = \left(\frac{Q_{\infty d} - Q_{id}}{\tau_d}\right) \exp\left[\frac{-t}{\tau_d}\right] \qquad (8)$$

where Q_{id} is the instantaneous accumulated charge on interfaces when the applied field is removed, $Q_{\infty d}$ is the final accumulated charge at the end of discharging time, and τ_d is a discharging relaxation time. Because charge can not change instantaneously, hence Q_{id} is equal to $Q_{\infty c}$. If τ_d is equal to τ_c and $Q_{\infty d}$ is zero, then the initial value of discharging current can be written as

$$I_d(0) = -\frac{Q_{id}}{\tau_d} = -\frac{Q_{\infty c}}{\tau_c} \approx -I_c(0) \qquad (9)$$

The measured results for $I_c(0)$ and $I_d(0)$ are $16.72\,\mu A$ [$I_{tc}(0) - I_s = I_c(0)$] and $-17.5\,\mu A$, respectively. This is almost in agreement with Equation 9.

Figure 5 shows the charging curves of the BSK sample measured at 1 V d.c. and 25° C for 50 ~ 95% r.h. From Fig. 5, it is found that: (1) the initial and final currents increase with increasing r.h.; (2) the initial current is far larger than the final current; (3) the initial current to final current ratio increases with increasing r.h. It means that there are two conduction carriers, ions and electrons, in this sample and the dominant conduction carrier of this sample in the humidity atmosphere is the ion. The increasing water vapour content can increase the concentrations of ions and electrons. Thus the total current of the sample on charging process follows Equation 7, where electron conduction current I_s and ion conduction charging current $I_c(t)$ increase with increasing r.h. As the applied voltage is constant (1 V) and the steady state current increases with increasing r.h., the value of R decreases with increasing r.h. This may be due to the effect that increasing water vapour can lower the activation energy of the sample [13], hence increasing the electron conductivity. The reason for initial charging current $I_c(0)$ increasing sharply at higher r.h. may be due to the following two factors: (1) $Q_{\infty c}$ increases with increasing r.h. as more water vapour can contribute more ions accumulating on the interfaces; (2) the charging relaxation time τ_c decreases with increasing r.h. The decrease of relaxation time τ_c with increasing r.h. may be due to the increase of ion conductivity at the grain surface, which can speed up ions arriving and accumulated at the electrode interface.

3.3. a.c. analysis and equivalent circuit model construction

To describe the a.c. electrical properties of materials, it can be expressed in any of three electrical parameters. These are complex admittance (Y), complex impedance (Z) and complex permittivity (ε^*). They have the following transformation relationships

$$\begin{aligned} Y(\omega) &= G(\omega) + jB(\omega) = Z(\omega)^{-1} \\ &= [Z'(\omega) + jZ''(\omega)]^{-1} \end{aligned} \qquad (10)$$

and

$$Y(\omega) = j\omega\varepsilon^* \frac{A}{d} = j\omega(\varepsilon' - j\varepsilon'')\frac{A}{d} \qquad (11)$$

where A and d are the cross-sectional area and thickness of the sample. The measured electrical parameters can be used to plot complex plane diagrams. Using complex plane plotting techniques can help in building the equivalent circuit model of the material. The establishment of equivalent circuit model must be simple and consistent with what is known about the physical processes [14], Seitz [15] gives eight rules to follow in model construction: (1) each significant conduction path must be represented by a parallel equivalent path; (2) each significant charge carrying species must be represented by parallel equivalent circuit paths; (3) each region of significance in a path must be represented by a lumped parameter circuit; (4) each mechanism of polarization must be represented by either a series or parallel combination of resistors and capacitors. Some types of polarization are: (a) electronic, (b) ionic, (c) lattice, (d) dipole, (e) orientation, (f) ferroelectric, (g) space charge (accumulated or depleted), (h) faradic (Warburg); (5) the "resistors" representing the various conducting species and "capacitors" representing polarization process, each has their own composition,

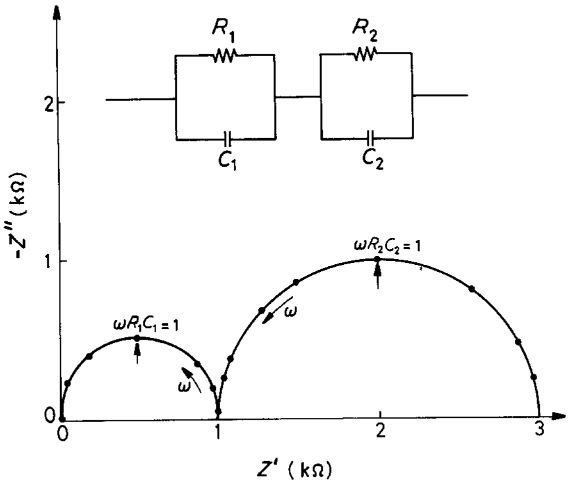

Figure 6 A network with $R_1 = 10^3\,\Omega$, $R_2 = 2 \times 10^3\,\Omega$, $C_1 = 1.6 \times 10^{-9}$ F, $C_2 = 2 \times 10^{-6}$ F, and its associated complex impeadance diagram.

microstructual, temperature and frequency dependences; (6) the paths of significance are those yielding the least impedence to current flow; (7) the regions of significance within these paths are those presenting the largest impediment to current flow; (8) complex plane plotting techniques can be used to elucidate an appropriate equivalent circuit representation from measured electrical quantities when used in conjunction with information obtained from other methods of study.

For example, the impedance of a parallel combination of an ideal resistance R and an ideal capacitance C can be written as

$$Z(\omega) = Z'(\omega) + jZ''(\omega)$$
$$= \frac{R}{1 + (\omega RC)^2} - j\frac{R^2 C_\omega}{1 + (\omega RC)^2} \quad (12)$$

From Equation 12, it will give an ideal semicircle passing through the origin in the complex impedance plane. This circuit is characterized by a single conductivity relaxation time τ, given by $\tau = RC$. The peak maximum of $-Z''$ occurs at a characteristic frequency given by $f_{\text{char}} = 1/2\pi\tau = 1/2\pi RC$. Figure 6 shows a network with two parallel R, C circuit in series and its associated complex impedance plot. It has two conductivity relaxation times given by $\tau_1 = R_1C_1$ and $\tau_2 = R_2C_2$ with $\tau_2 \gg \tau_1$, hence the total conductivity relaxation time, τ_s, of this circuit is approximated as

$$\tau_s = \tau_1 + \tau_2 \approx \tau_1 \quad (13)$$

Unfortunately, the typically observed complex plane plots for many solid ionics and dielectrics have either inclined semicircles with their centres depressed below the real axis by an angle of $\alpha\pi/2$ or spurs which are inclined to the vertical axis by an angle of $\alpha\pi/2$. These kind of "non-Debye" behaviour can not be described in terms of Debye equations, and have been explained by many authors [9, 16, 17]. Von—Schweidler [16] ascribes the "non-Debye" behaviour to the distribution of relaxation times which arise from the difference in the local environments of the dipoles. An lumped circuit element Warburg impedance is used to represent the distributed network, but complex planes so obtained will give only a 45° inclined angle. Thus it can not explain the most experiments. Macdonald [17] ascribes the entire frequency dependence of the impedance data to an interfacial process at the electrodes and at internal grain boundaries which limit the transparency of these barriers to different ionic species. A set of complicated equations is developed from which complex plane diagrams are generated. The complex plane so obtained have their centres depressed below the real axis by different amounts without the need of multiple relaxation times, but it is rigorous and is not fit for practical utility. Jonscher [8] observes an "universal" dielectric response of many solid materials. He proposes a dispersive frequency-dependent "non-Debye" capacitance $C_n(\omega)$ to account for the empirical observed shape of the inclined complex plane diagrams. It is verified that the complex plane diagrams obtained by the equivalent circuit model associated with "non-Debye" capacitance have their centres depressed below the real axis by different angle. The "non-Debye" capacitance is given by the relation

$$C_n(\omega) = C(j\omega)^{n-1} \quad (14)$$

where $j = \sqrt{-1}$ and $n = 1 - \alpha$. Using this relation, it can be derived out that the impedance of a parallel combination of an ideal conductance G with an "non-Debye" capacitance $C_n(\omega)$ can be expressed as follows

$$Z(\omega) = [Y(\omega)]^{-1} = [G + C(j\omega)^n]^{-1}$$
$$= Z'(\omega) - jZ''(\omega) \quad (15)$$

with

$$Z'(\omega) = \frac{G + C\left[\cos\frac{n\pi}{2}\right]\omega^n}{\left[G + C\left(\cos\frac{n\pi}{2}\right)\omega^n\right]^2 + \left[C\left(\sin\frac{n\pi}{2}\right)\omega^n\right]^2} \quad (16)$$

and

$$Z''(\omega) = \frac{C\left[\cos\frac{n\pi}{2}\right]\omega^n}{\left[G + C\left(\cos\frac{n\pi}{2}\right)\omega^n\right]^2 + \left[C\left(\sin\frac{n\pi}{2}\right)\omega^n\right]^2} \quad (17)$$

Figure 7 shows the complex impedance plots of BSK sample at 25° C for 65 ~ 95% r.h. They appear to have semicircles with their centres depressed below the real axis by an angle of $\alpha_2\pi/2$ and pass through or close to the origin at sufficiently high frequencies. At lower frequencies, these semicircles go over into what appear to be the beginning of another inclined semicircles and incline to the real axis by an angle of $n_1\pi/2$. But these low frequencies inclined semicircles are not sufficiently developed in the available range of frequencies. From these plots, it is found that the high frequency inclined angle $\alpha_2\pi/2$ decreases with increasing r.h. Yet the characteristic frequency f_{charH}, assuming which is occurred at the peak maximum of $-Z''$,

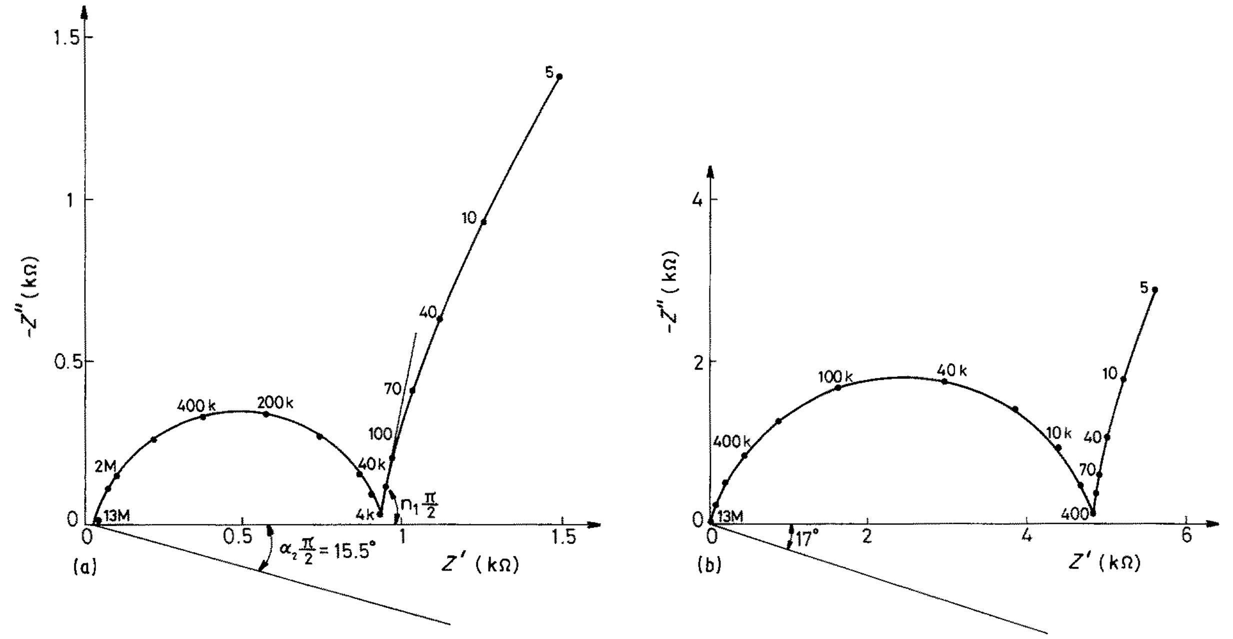

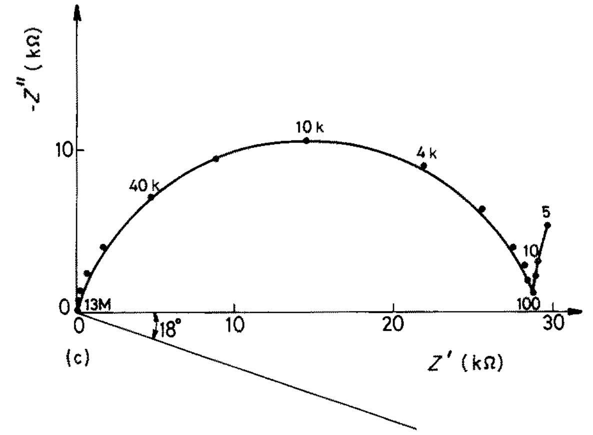

Figure 7 The complex impedance plots of BSK sample at 25° C and different r.h. (a) 95%; (b) 80%; (c) 65%.

increases with increasing r.h. Besides, it seems to have a tendency that there is another characteristic frequency f_{charL} at very low frequency (below 5 Hz) with $f_{\text{charL}} \ll f_{\text{charH}}$, and f_{charL} increases with increasing r.h. If f_{char} approximates $1/2\pi\tau$ as ideal semicircle given, then the total conductivity relaxation time can be approximated as

$$\tau_s = \tau_L + \tau_H \approx \frac{1}{2\pi}\left(\frac{1}{f_{\text{charL}}} + \frac{1}{f_{\text{charH}}}\right) \approx \frac{1}{2\pi}\left(\frac{1}{f_{\text{charL}}}\right) \tag{18}$$

Thus the total conductivity relaxation time will be dominated by lower characteristic frequency f_{charL}, and the total conductivity relaxation time τ_s is inversely proportional to f_{charL}. Increasing r.h. can have a larger f_{charL}, so τ_s decreases with increasing r.h., which is agreed with the d.c. analysis result.

Figure 8 shows the equivalent circuit model for BSK sample in humidity atmosphere. In this model, the sample is separated into three regions: crystal grain, grain surface and electrode surface, where R_g, R_{gs}, C_{gsn}, R_e and C_{en} represent the crystal grain resistance, grain surface resistance, grain surface "non-Debye" capacitance, electrode surface resistance and electrode surface "non-Debye" capacitance, respectively. Using this equivalent circuit model, and let the "non-Debye" capacitances to be

$$C_{en} = C_1(j\omega)^{n_1-1} \quad \text{and} \quad C_{gsn} = C_2(j\omega)^{n_2-2} \tag{19}$$

then the impedance of this model can be written as follows

$$Z(\omega) = Z'(\omega) - jZ''(\omega) \tag{20}$$

with

$$Z'(\omega) = R_g + \frac{\frac{1}{R_{gs}} + C_2\left[\cos\left(\frac{n_2\pi}{2}\right)\right]\omega^{n_2}}{\left[\frac{1}{R_{gs}} + C_2\left(\cos\frac{n_2\pi}{2}\right)\omega^{n_2}\right]^2 + \left[C_2\left(\sin\frac{n_2\pi}{2}\right)\omega^{n_2}\right]^2} + \frac{\frac{1}{R_e} + C_1\left[\cos\left(\frac{n_1\pi}{2}\right)\right]\omega^{n_1}}{\left[\frac{1}{R_e} + C_1\left(\cos\frac{n_1\pi}{2}\right)\omega^{n_1}\right]^2 + \left[C_1\left(\sin\frac{n_1\pi}{2}\right)\omega^{n_1}\right]^2} \tag{21}$$

and

$$Z''(\omega) = \frac{C_2\left[\sin\left(\frac{n_2\pi}{2}\right)\right]\omega^{n_2}}{\left[\frac{1}{R_{gs}} + C_2\left(\cos\frac{n_2\pi}{2}\right)\omega^{n_2}\right]^2 + \left[C_2\left(\sin\frac{n_2\pi}{2}\right)\omega^{n_2}\right]^2} + \frac{C_1\left[\sin\left(\frac{n_1\pi}{2}\right)\right]\omega^{n_1}}{\left[\frac{1}{R_e} + C_1\left(\cos\frac{n_1\pi}{2}\right)\omega^{n_1}\right]^2 + \left[C_1\left(\sin\frac{n_1\pi}{2}\right)\omega^{n_1}\right]^2} \tag{22}$$

using Equations 21 and 22, the simulation parameter values of the BSK sample under 65 ~ 95% r.h. are listed in Table II. It is verified [18] that the simulation results using these parameters values fit very well with the measured results. In Table II, it indicates that: (1)

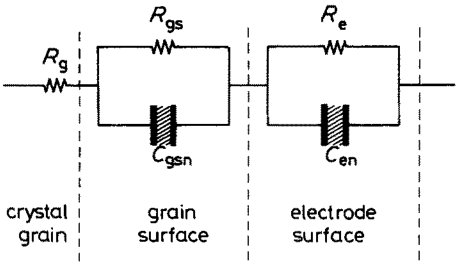

Figure 8 The equivalent circuit model of BSK sample.

R_{gs} and R_e decrease with increasing r.h.: (2) C_1 and C_2 increase with increasing r.h.; (3) R_g does not affect by the variation of r.h. These can be interpreted as follows:

1. When little water vapour is present, a water molecule will be physically adsorbed on an activated site to form an hydroxyl group on the grain surface, and a proton may be transferred from a surface hydroxyl group to a water molecule to form H_3O^+. In this condition, (adsorbed layer less than one monolayer) each water molecule is bonded to two hydroxyl groups and the dominant charge carriers will be H_3O^+. When more water is adsorbed (greater then one monolayer), clustering of the water molecules takes place forming patches of an ice-like layer of hydrogen-bonded water molecules, and each water molecule is only singly bonded to a hydroxyl group [4]. Since hydration of H_3O^+ into H_2O and H^+ is energetically favoured in liquid water [19], so the dominant charge carrier in high moisture atmosphere is H^+ (proton). The concentrations of H^+ increase with increasing water vapour and H^+ can move freely in liquid water, the result is the decrease of grain surface resistance R_{gs} with increasing r.h.

2. Water molecules with two surface hydroxyl bonding (low humidity state) will not be as free to reorient in an applied electric field as those which are singly bonded (high humidity state). Thus the singly bonded H_2O will make a greater contribution to the dielectric constant then doubly bonded H_2O [4], and the water molecule polarization effect is enhanced with increasing water vapour. The result is the increase of C_2 with increasing r.h.

TABLE II Simulation parameter values of BSK sample at 25°C and 65 ~ 95% r.h.

Relative humidity (%)	R_g (Ω)	R_{gs} (Ω)	C_1 (μF)	C_2 (nF)	n_1	n_2	L (μH)	R_e (kΩ)
95	25	897	19.0	7.5	0.867	0.82	0.35	7
80	25	4827	13.0	7.0	0.880	0.81	0.35	700
65	25	29000	8.5	6.0	0.880	0.79	0.35	70000

3. From d.c. analysis, the blocking electrode can accumulate charged ions to cause space charge polarization which appears as an increase in capacitance. Increasing r.h. can cause more charges to accumulate on the electrode surface, hence increasing the value of C_1.

4. The conduction carriers of the sample in moisture atmosphere are ion and electron. The electron carriers can pass through or arrive at the electrodes. Thus, the electrode surfaces is represented by parallel combination of R_e and C_{en}, where R_e denotes the resistivity of electron at electrode surface which decreases with increasing water vapour for increasing r.h. can lower the activation energy of the sample.

5. The crystal grain does not react with water vapour, hence R_g is not affected by r.h.

References

1. T. NITTA and S. HAYAKAWA, *IEEE Trans. Components, Hybrids, Manuf. Technol.* **CHMT-3** (1980) 237.
2. Y. SADAOKA, M. MATSUGUCHI, Y. SAKAI, H. AONO, S. NAKAYAMA and H. KUROSHIMA, *J. Mater. Sci.* **22** (1987) 3685.
3. TATSUO, YAMAMOTO, and H. SHIMIZU, *IEEE Trans. Components, Hybrids, Manuf. Technol.* **CHMT-5** (1982) 238.
4. J. H. ANDERSON and G. A. PARKS, *J. Phys. Chem.* **72** (1968) 3362.
5. E. McCAFFERTY and A. C. ZETTLEMOYER, *Discuss Farady Soc.* **52** (1971) 239.
6. Y. SHIMIZU, M. SHIMABUKURO, H. ARAI and T. SEIYAMA, *Chem. Lett.* (1985) 917.
7. Y. C. YEH and T. Y. TSENG, *J. Mater. Sci. Lett.* **7** (1988) 766.
8. A. K. JONSCHER, *J. Mater. Sci.* **13** (1978) 553.
9. A. K. JONSCHER, *Phys. Status Solidi (a)* **32** (1975 665.
10. W. J. LO, Y. W. CHUNG and G. A. SOMORJAI, *Surf. Sci.* **71** (1978) 199.
11. P. A. THIEL and T. E. MADEY, *Surf. Sci. Reports* **7** (1987) 211.
12. W. D. KINGERY, H. K. BOWEN and D. R. UHLMANN, "Introduction to ceramics" (John Wiley and Sons, New York, 1977) p. 922.
13. K. TENNAKONE, *J. Chem. Soc., Farady Trans. 1* **79** (1983) 705.
14. J. E. BAUERLE, *J. Phys. Chem. Solids* **30** (1969) 2657.
15. M. A. SEITZ, *Internat. J. Hybrid Microelectronics* **3** (1980) 7.
16. E. V. SCHWEIDLER, *Ann. d. Physik.* **24** (1907) 711.
17. J. R. MACDONALD, *J. Chem. Phys.* **58** (1973) 4982.
18. Y. C. YEH and T. Y. TSENG, accepted for publication *IEEE Trans. Components, Hybrids, Manuf. Technol.*
19. R. W. GURNEY, "Ionic processes in solution" (McGraw Hill, New York, 1953).

Received 31 August
and accepted 18 November 1988